Journal of Nuclear Materials 390–391 (2009) 947–950

Contents lists available at ScienceDirect

Journal of Nuclear Materials

journal homepage: www.elsevier.com/locate/jnucmat

Power deposition modelling of the ITER-like wall beryllium tiles at JET

M. Firdaouss [a,e,*], R. Mitteau [b,e], E. Villedieu [c,e], V. Riccardo [c,e], P. Lomas [c,e], Z. Vizvary [c,e], C. Portafaix [b,e], L. Ferrand [a,e], P. Thomas [b,e], I. Nunes [c,e], P. de Vries [c,e], P. Chappuis [d,e], Y. Stephan [a,e]

[a] Assystem, 23 rue Benjamin Franklin, 84120 Pertuis, France
[b] Association Euratom-CEA, CEA/Direction des Sciences de la Matière, Département de Recherches sur la Fusion Contrôlée, Centre de Cadarache, 13108 Saint-Paul-Lez-Durance, France
[c] UKAEA/Euratom Fusion Association, Culham Science Centre, Abingdon, Oxfordshire OX14 3DB, UK
[d] ITER, JWS Cadarache, Centre de Cadarache, 13108 Saint-Paul-Lez-Durance, France
[e] JET-EFDA, Culham Science Centre, OX14 3DB Abingdon, UK

ARTICLE INFO

PACS:
07.05.Tp
28.52.Av
44.90.+c
52.40.Hf

ABSTRACT

A precise geometric method is used to calculate the power deposition on the future JET ITER-Like Wall beryllium tiles with particular emphasis on the internal edge loads. If over-heated surfaces are identified, these can be modified before the machining or failing that actively monitored during operations. This paper presents the methodology applied to the assessment of the main chamber beryllium limiters. The detailed analysis of one limiter is described. The conclusion of this study is that operation will not be limited by edges exposed to plasma convective loads.

1. Introduction

ITER will use beryllium as plasma facing material in the main chamber, as this material has several advantages compared to carbon, which is the material more commonly used now. This is an important innovation as the quantity and the surface of Be involved will be large. To prepare for the ITER wall, JET is planning the complete replacement of its present CFC main wall by Be and its present divertor by tungsten, as part of the ITER-Like Wall (ILW) project [1]. The position and global shape of the poloidal limiters are not modified with respect to the present ones. Most of the modifications are in the tiles [2]. Each tile is composed of several slices and each slice is castellated. This particular design ensures the reduction of the Eddy currents and thermal stresses. The counterpart of this is the potential exposure of poloidal-facing and toroidal-facing faces (named thereafter poloidal and toroidal faces) to very high heat fluxes, leading to potential melting of the Be into the chamber and pollution of the plasma [3]. The tile surfaces have also been modified to shadow the edges from near perpendicular field lines, by introducing ski-slopes. However, this is not possible everywhere, and field line penetrations can occur locally in the castellation and sub-assembly gaps or between the tiles. Therefore, it is necessary to quantify the power deposited on these penetrations and compare it with the incident heat flux on the tile front face.

The power deposition pattern onto all main wall components has to be performed under realistic plasma conditions as in the later ILW operation. A purely parallel heat flux deposition code has been developed by CEA, and successfully contributed to the CIEL project design [4,5]. It was then adapted to JET (JETFLU) [6,7]. The parallel modelling neglects the effects of the Larmor radius and the imbalance between the ion and electronic sides; hence the power flux conducted along the field line penetration is probably overestimated. The principal advantage of this code is its flexibility, which allows computing heat flux pattern for any surface in any magnetic configuration. This means that the computed surface can be as close to the real one as required.

This paper describes the concepts and the methodology applied in the heat flux computations in Section 2. The Section 3 gives a detailed example of the analysis of the wide poloidal limiter, as well as a short summary of the results. Section 4 gives the general assessment of the behaviour of the ILW Be tiles in the plasma configurations studied, and describes possible additional analysis.

2. Methods

Several inputs are required to calculate shadowing and incident heat flux on a given surface. The shadowed surface, on which shadowing is computed, is meshed by a finite element modelling software. This mesh can be refined on the edges and areas of steep gradient. This is done with CATIA v5 software, as the design office models are made with it. A second mesh is done for the shadowing surface, which is the limiter surface supposed to protect the shadowed surface.

The magnetic configuration is defined on a grid, and the magnetic field is supposed to be invariant by rotation. The magnetic

* Corresponding author. Address: Assystem, 23 rue Benjamin Franklin, 84120 Pertuis, France.
E-mail address: mfirdaouss@assystem.com (M. Firdaouss).

0022-3115/$ - see front matter © 2009 Elsevier B.V. All rights reserved.
doi:10.1016/j.jnucmat.2009.01.243

field vector and poloidal flux are defined on each node of the grid, as provided by Proteus [8], a magnetic equilibrium code. Proteus computes also the incident heat flux on the nodes of a given reference surface below the shadowed mesh. This surface is used in the incident heat flux calculation.

At each step of the calculation, the nodes of the shadowed mesh are moved following the direction of the magnetic vector by the length of ascent, typically less than 5 mm. Then a test is done to determine if the field line intersects the shadowing mesh. If it does, the initial node is shadowed; if not the process reiterates until the maximal connexion length (roughly the distance between the shadowing and shadowed meshes) is reached, meaning that the initial node is wetted by the plasma. This process is illustrated in Fig. 1. The resulting shadowing mask is shown in Fig. 2.

The incident heat flux is computed by a similar process, an algorithm calculates the intersection of each field line coming from the nodes with the reference line. This gives the heat flux along each field line, and it is then scaled according to the angle of incidence on each node. Power deposition is then combined with the shadowing mask to obtain the deposition pattern (Fig. 2).

A first computation is done on a whole given limiter, allowing determining the most loaded tiles. They are then computed again with a smaller mesh size. If needed, a third computation is done at the castellation scale including the internal faces, with an even smaller mesh size again. This way minimises the number of computations while the most heated, and thus most limiting, areas are still checked. Finally, a simple thermal computation is done to estimate the local temperature increase, by summing the temperature increases computed separately on each wetted face (approximated as a semi-infinite slab for the front face and a strip heating for the others). The resulting temperatures are indicative, and are used essentially to compare thermal loads at different scales.

A semi-analytical code has been used by JET to define the surface of the tiles [2]. This code can also compute the heat flux under the assumption of a cylindrical plasma and a cylindrical wall. Before assessing the ILW limiters, a benchmark has been successfully performed to prove the accuracy of JETFLU.

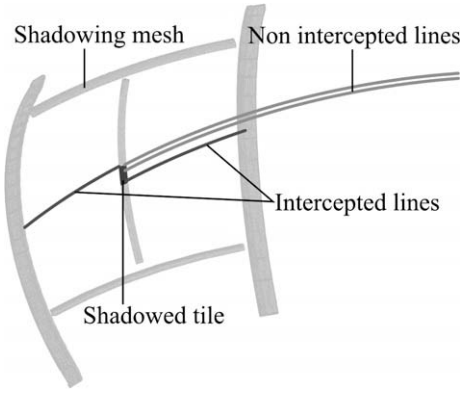

Fig. 1. ICRH antenna: examples of field lines coming from the septum partially shadowed by the private limiter.

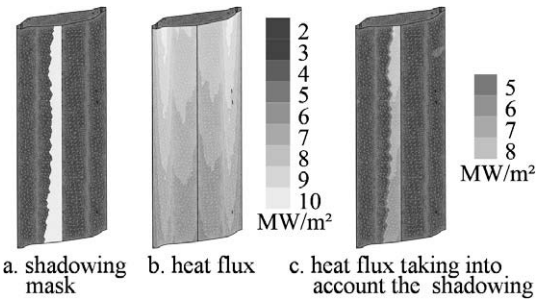

Fig. 2. Heat flux deposition calculated from shadowing mask and heat flux.

3. Results

All the main chamber Be assemblies have been analysed with JETFLU. Five limiter equilibria have been chosen for checking, with the assumption of 10 MW lost by the plasma during a 10 s contact. The power decay length is $\lambda_q = 1.0$ cm at the outside mid-plane [9].

This work has necessitated several hundreds of calculations. Only a sample computation case is presented, along with a table summarizing the main results obtained for the heat flux computation on the wide Poloidal Limiter (wPL). The magnetic configuration used is the most extreme limiter plasma, designed to be close to all in vessel components.

The wPL is the main poloidal limiter for the low field side. This limiter defines the last closed flux surface for the studied magnetic configurations, and can be subject to very high power densities.

The shadowing is considered coming from the two closest neighbouring wPL. The wPL chosen for the assessment is the one with the largest distance to the neighbouring limiters. Fig. 3 shows the incident heat flux taking into account the computed shadowing. As explained above, the first step is to identify the most heated tiles for the whole limiter. The most heated tile is 22, counting from the bottom (1 m above the outside mid-plane). The second step is to compute a more precise heat flux deposition pattern on this tile. The mesh is refined, and neighbouring tiles are added to the neighbouring wPL as shadowing surfaces. The computation shows that the left part is well shadowed (Fig. 3), but the right part receives heat fluxes up to 9.5 MW m^{-2}. This gives a temperature increase of 1570 °C.

Moreover, some heat flux is deposited on the right of the upper poloidal face: the upper tile does not shadow completely the top face of the tile 22. The penetration length is 2.5 mm with a heat flux of 2.5 MW m^{-2}, whereas the local front heat flux is 7 MW m^{-2} (Fig. 3). This gives a local temperature increase of 1290 °C, which is lower than the temperature increase associated to the maximal front heat flux.

The last step is to calculate shadowing and heat fluxes around the maximal front heat flux, as the castellation could cause a strong overheating. The most heated castellation is meshed very finely, especially the toroidal face. The neighbouring castellations are added to the shadowing surfaces. Fig. 3 includes a sketch of the power deposition pattern on the most exposed castellation. As expected, all three faces; front, poloidal and toroidal, are wetted. The front face heat flux is 9.3 MW m^{-2}. On the poloidal face, the penetration length is 0.29 mm and the heat flux is 11.3 MW m^{-2}. On the toroidal face the values are 0.06 mm and 78 MW m^{-2}, respectively. Because the front heat flux is close to the maximal front heat flux, the temperature increase on this corner is higher: 1870 °C. This is acceptable, given that the 82% of the temperature increase originates the front power density. The power density on the toroidal face accounts for 11% and the power density on the poloidal face for 7%.

The conclusion in this sample case is that the front surface heat flux is primarily responsible of the tile heating. The overheating

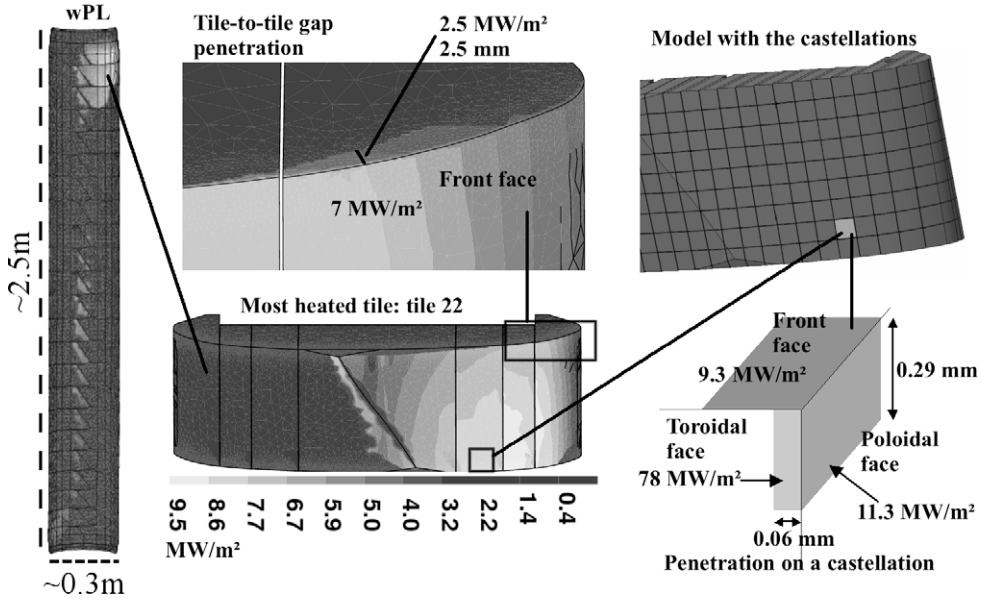

Fig. 3. Heat flux computation from the limiter scale to the castellation.

Table 1
Synthesis of the power deposition calculation on the wPL in four magnetic configurations.

Tile	Case	Type of deposition	Total temp	Front flux	Front %T	Pol flux	Pol length	Pol %T	Tor flux	Tor length	Tor %T
22	3610006	Castellation	1870	9.3	82	11.3	0.29	7	78	0.06	11
12	3610005	Castellation	1730	8.4	80	18.4	0.26	11	111	0.03	9
12	3610003	Front face	1600	9.7	100						
22	3610006	Front face	1570	9.5	100						
12	3610005	Front face	1440	8.7	100						
22	3610006	Tile to tile gap	1290	7	89	2.5	2.5	11			
15	3610004	Front face	1240	7.5	100						
22	3610005	Front face	1240	7.5	100						
22	3610005	Tile to tile gap	1020	5.5	89	2	2.5	11			
2	3610006	Front face	830	5	100						
22	3610004	Front face	280	1.7	100						
2	3610005	Front face	170	1	100						

due to the faces of the castellations and to the inter-tiles gaps is marginal compared to the benefits of this particular design.

The same analysis as detailed above is performed in four different magnetic configurations. Table 1 presents the results obtained. Each row shows the maximal temperature increase caused by the power deposition in different places. First column is the number of the tile as defined above. Second column is the reference number of the magnetic equilibrium used. The type of deposition indicates if the power deposition is on the front face, inside a gap between neighbouring tiles or inside the tile, on a castellation. The following column is the total temperature increase caused by the heat flux. Next columns give the heat fluxes for each face (front, poloidal and toroidal), as well as the penetration length for the poloidal and toroidal faces. The '%T' columns give the relative part of the temperature increase caused by a face to the total temperature increase. The temperatures are given in °C, the heat fluxes in MW m^{-2} and the lengths in mm.

The most heated areas are obviously the castellations. Indeed, the front power density on a castellation is close to the maximal front power density of the tile. And with the heating caused by the poloidal and toroidal faces, the temperature increase can only be higher. But for both computed castellation, the temperature increase is dominated by the power deposition on the front face (around 80%). The supplementary temperature increase caused by the castellations is marginal.

4. Conclusion

This study has shown the possibility to precisely predict the heat load on the JET ILW Be tiles for several plasma configurations. The design complexity due to the new sliced and castellated Be tile assemblies has greatly increased the difficulty to estimate the power loads. The methodology applied in this assessment is both precise and efficient at computing power deposition and shadowing on critical tiles.

The additional heating caused by the penetrating field lines is small (generally less than 20%) compared to the main face heat flux. This means that operation will be primarily limited by the front face heat flux and confirms that the design suits the requirements. However, the temperature increase allowed is only around 800 °C, as some margin needs to be preserved (the Be melting point is 1280 °C and the device temperature is 200 °C). The operator will need to introduce protection mechanisms to avoid overheating by means of passive and/or active monitoring.

References

[1] G.F. Matthews et al., J. Nucl. Mater. 390–391 (2009) 934.
[2] I. Nunes, P. de Vries, P.J. Lomas, Fusion Eng. Des. 82 (2007) 1846.

[3] A. Loarte et al., J. Nucl. Mater. 337–339 (2005) 816.
[4] R. Mitteau et al., J. Nucl. Mater. 266–269 (1999) 798.
[5] R. Mitteau et al., J. Nucl. Mater. 313–316 (2003) 1229.
[6] Ph. Chappuis et al., Fusion Eng. Des. 75–79 (2005) 413.
[7] J.-F. Salavy et al., Fusion Eng. Des. 75–79 (2005) 505.
[8] R. Albanese, J. Blum, O. DeBarbieri, in: Proceedings of 12th Conference on the Num. Sim. of Plasmas San Francisco, CA, USA, 1987, p. IT4.
[9] A. Loarte et al., J. Nucl. Mater. 266–269 (1999) 587.